# An estimate of the dispersion of repolarization times based on a biophysical model of the ECG

Roberto Sassi, *Member, IEEE,* and Luca T Mainardi

***Abstract*—Temporal heterogeneity of ventricular repolarization is a key quantity for the development of ventricular reentrant arrhythmia. The paper introduces the $\mathcal{V}$-index, a novel electrocardiogram (ECG)-based estimator of the standard deviation of ventricular myocytes' repolarization times $s_\vartheta$. Differently from other ECG metrics of repolarization heterogeneity, the $\mathcal{V}$–index was derived from the analysis of a biophysical model of the ECG, where repolarization is described by the Dominant T-wave (DTW) paradigm. The model explains the shape of T waves in each lead as a projection of a main waveform (the DTW) and its derivatives weighted by scalars, the lead factors.**

**A mathematical formula is derived to link the heterogeneity of ventricular repolarization $s_\vartheta$ and the $\mathcal{V}$–index. The formula was verified using synthetic 12-Leads ECGs, generated with a direct electrophysiological model for increasing values of $s_\vartheta$ (in the range 20 to 70 ms). A linear relationship between the $\mathcal{V}$–index and $s_\vartheta$ was observed, $\mathcal{V} \approx 0.675\ s_\vartheta + 1.8$ ms ($R^2 = 0.9992$).**

**Finally, 68 ECGs from the E-OTH-12-0068-010 database of the Telemetric and Holter ECG Warehouse (THEW) were analyzed. The $\mathcal{V}$–index coherently increased after sotalol administration, a drug know to have QT-prolonging potential ($p \ll 0.001$).**

***Index Terms*—Repolarization heterogeneity, Statistical modeling of repolarization times, Cardiac transmembrane potentials, T wave analysis, Dominant T Wave**

## I. Introduction

SPATIAL dispersion of ventricular repolarization is a property of the human heart and it is responsible for the genesis of the T–wave on the Electrocardiogram (ECG). However, an amplification of such dispersion creates suitable conditions for the mechanism of reentry and favors the development of ventricular tachicardia/fibrillation [1], [2]. Therefore, being able to assess repolarization heterogeneity from the ECG would be of clinical value for the prognosis of ventricular life-threatening arrhythmia and cardiovascular side-effects of drugs [3]. Unfortunately, this is still an open challenge [4].

Several metrics related to T–wave morphology (amplitude, width [5], nondipolar components [6]) and duration (QT dispersion [7] and $T_{apex}$–$T_{end}$ [8], [9]) have been proposed to quantify repolarization heterogeneity. Although they proved to have prognostic significance, it is unclear to what extent they are representative of the repolarization heterogeneity and of its origin (apico–basal, transmural, local or global). An issue is that these indexes were validated on animal observations (or in coronary perfused wedge preparations), but extrapolation to *in vivo* human ECG recordings is not straightforward [10]. As a result, when applied to human recordings, they showed limitations [11], [4], have been questioned [12] or provided controversial interpretations [10], [13], [14]. Only recently, their validation through computer–simulated ECG models was performed [15], [6]. While these studies quantified the sensitivity of each index to repolarization heterogeneity, they did not explain their physical link with repolarization dispersion. Therefore the quantification of repolarization heterogeneity, via methods which are explicitly linked to a physical model of myocardial repolarization, is still missing.

Moving from this scenario, we derived a novel method to quantify the dispersion of myocytes' repolarization times, rooted on a biophysical model of the ECG. The heart and the thorax were described using the classical Geselowitz approach [16]. Then we built on the Dominant T-wave formalism (DTW), first implied by van Oosterom [17]. The weights, which modulate the DTW to generate the T–wave of each lead, are known as *lead factors* [18]. We will show that the variability of lead factors across successive beats is related to the standard deviation of the repolarization times.

## II. Modeling background

The *bidomain model* describes the time evolution of the electrical properties of the myocardial muscle. It was developed independently by several authors: Geselowitz and Miller [19], Tung [20] and possibly others, but the original suggestion of having "interpenetrating domains" is in the work of Schmitt [21]. In the bi-domain model, the cardiac tissue is made up of two distinct and separate domains, modeling the intracellular and extracellular space, which share the same volume. Each domain acts like a regular volume conductor with the difference that in each point two potentials and currents are defined. It is a continuous model and it does not take into account the individual cells.

The bi-domain model is commonly employed in large scale simulations, see for example [22]. In here, similarly to Geselowitz [23], we focus on the resulting potentials produced at the body surface. This constitutes a volume conductor problem also, where the conductor (inhomogeneous) is constituted by the torso. In the frequency spectrum of interest ($\leq 1000$ Hz) the problem can be safely considered quasi-static and the potential $\psi$ collected by an ECG lead is given by

$$\psi = -\int_{\mathcal{H}} c_i \nabla \phi_m \cdot \nabla Z \mathrm{d}v \qquad (1)$$

where $c_i$ is the inner domain conductance tensor, $\phi_m$ is the transmembrane potential (cell's interior minus exterior

L.T. Mainardi is with the Dipartimento di Bioingegneria, Politecnico di Milano, Piazza Leonardo da Vinci 32, 20133 Milan, Italy.

R. Sassi is with the Dipartimento di Tecnologie dell'Informazione, Università degli Studi di Milano, Via Bramante 65, 26013 Crema, Italy (corresponding author, e-mail: roberto.sassi@unimi.it)

Manuscript received March 8, 2011. 

potential) and $\nabla Z$ is the transfer impedance function, relating the current dipole $c_i \nabla \phi_m$ in the volume $\mathrm{d}v$ with the potential it generates in the lead. The integral is performed over the volume of the heart $\mathcal{H}$. When the anisotropy ratio of the inner and outer domains are the same, the integral in (1) is equivalent [16] to

$$\psi = -\int_{\mathcal{S}} c_i \phi_m \nabla Z \cdot \mathrm{d}\vec{s} \tag{2}$$

where $\mathcal{S}$ is the surface enclosing the active region of the heart (endocardium, epicardium and septum). Cardiac tissue does not satisfy the equal anisotropy condition quite well. Nevertheless, according to the results in Plonsey & Barr [24] for a two-dimensional anisotropic cardiac tissue, the equal anisotropy ratio approximation practically holds, except close to the site of activation.

Given that the integral in (2) is taken only over the surface $\mathcal{S}$, the active sources in the heart may be substituted, with no effect on $\psi$, by a dipole layer on $\mathcal{S}$ with a moment proportional to $\phi_m$. This is often called "(equivalent) surface source model" and it links the potential in a lead with the cellular transmembrane action potential at the surface $\mathcal{S}$.

### A. The DTW formalism

Van Oosterom [17] noticed that when employing equation (2) to solve the forward electrocardiographic problem during repolarization, i.e. simulating surface ECG from the heart electrical activity, one in practice evaluates a linear system at each time step[1]. First the heart surface is subdivided in $M$ contiguous regions ("nodes") where the sources are lumped together. Then, one approximates (2), at any instant $t$, with

$$\begin{bmatrix} \psi_1(t) \\ \cdots \\ \psi_L(t) \end{bmatrix} = \boldsymbol{\psi}(t) = \mathbf{A} \begin{bmatrix} D_1(t) \\ \cdots \\ D_M(t) \end{bmatrix}, \tag{3}$$

where $\boldsymbol{\psi}(t)$ is a vector of potentials (one for each of the $L$ leads considered) and $\mathbf{A}$ is a transfer matrix. Matrix $\mathbf{A}$ has size $[L \times M]$ and it is fixed for a given subject and a specific leads configuration. It accounts for both the volume conductor (geometry and conductivity) and the solid angle under which the single source contributes to the potentials in $\boldsymbol{\psi}$. The functions $D_m(t)$ describes the repolarization phase of the transmembrane potentials (TMP) of the myocytes of a given region. From geometrical considerations, the sum of the elements of each row of the matrix $\mathbf{A}$ vanishes. Equivalently $\mathbf{A}\mathbf{e}_1 = 0$ where $\mathbf{e}_1$ is a $[M, 1]$ vector whose elements are all set to 1. The property of $\mathbf{A}$ evidences that there is a surface T-wave only if the functions $D_m(t)$ differ.

Van Oosterom [17] then pointed out that it was possible from equation (3) to link the shape of the T wave in each lead to the transmembrane potential. In fact, making the further approximation that the only difference across different $D_m(t)$ functions is the repolarization time (RT) $\rho_m$, that is $D_m(t) = D(t - \rho_m)$, then

$$\boldsymbol{\psi}(t) = \mathbf{A} \begin{bmatrix} D(t-\rho_1) \\ \cdots \\ D(t-\rho_M) \end{bmatrix}. \tag{4}$$

[1]The linearity comes from the linear conductive properties of the torso as a volume conductor.

The RT $\rho_m$ is defined here as the instant in time at which the downslope of the TMP $D(t)$ is maximum. The approximation is not severe and substantially states that the TMP downslope is approximately constant across the surface of the heart.

The RT of each node may be equivalently expressed as $\rho_m = \bar{\rho} + \Delta\rho_m$ where $\bar{\rho} = \sum_{m=1}^{M} \rho_m / M$ is the average repolarization time. When $\Delta\rho_m \ll \bar{\rho}$, the function $D(t)$ can be expanded in series around $\bar{\rho}$ leading to

$$\begin{aligned} D(t-\rho_m) = D(t-\bar{\rho}) - \Delta\rho_m \left.\frac{dD(\tau)}{d\tau}\right|_{\tau=t-\bar{\rho}} \\ + \frac{\Delta\rho_m^2}{2!} \left.\frac{d^2D(\tau)}{d\tau^2}\right|_{\tau=t-\bar{\rho}} + o(\Delta\rho_m^3). \end{aligned} \tag{5}$$

Given the fact that $\mathbf{A}e_1 D(t-\bar{\rho}) = 0$ and neglecting higher order terms, the model in equation (4) can be recast into

$$\boldsymbol{\psi}(t) \approx -\mathbf{A}\Delta\boldsymbol{\rho}\dot{D}(t-\bar{\rho}), \tag{6}$$

where $\Delta\boldsymbol{\rho} = [\Delta\rho_1, \Delta\rho_2, \ldots, \Delta\rho_M]^T$, or, in discrete–time

$$\boldsymbol{\Psi} \approx \boldsymbol{w}_1 \mathbf{T}_d,$$

where $\boldsymbol{w}_1 = -\mathbf{A}\Delta\boldsymbol{\rho}$ is the $[L \times 1]$ vector of *lead factors*, $\boldsymbol{\Psi}$ is a $[L \times N]$ matrix containing the $N$ ECG samples recorded from $L$ leads and $\mathbf{T}_d$ is a $[1 \times N]$ vector obtained after sampling $\dot{D}(t)$. The quantity $-\mathbf{T}_d$ was termed by van Oosterom *dominant* T-wave[2] [25]. In fact, when the approximation in equation (5) holds, the single T-waves measured on different leads are only a scaled version of $\mathbf{T}_d$. Methods suitable for the computation of $\mathbf{T}_d$ and $\boldsymbol{w}_1$ are briefly reviewed in Appendix A.

When the dispersion of the repolarization times increases, as it is speculated for example with ventricular tachycardia [26], the expansion in equation (6) breaks down and higher order contributions become relevant. A second order approximation of equation (4) is

$$\begin{aligned} \boldsymbol{\psi}(t) &\approx -\mathbf{A}\Delta\boldsymbol{\rho}\dot{D}(t-\bar{\rho}) + {}^1\!/_2\mathbf{A}\Delta\boldsymbol{\rho}^2\ddot{D}(t-\bar{\rho}) \\ \boldsymbol{\Psi} &\approx \boldsymbol{w}_1\mathbf{T}_d + \boldsymbol{w}_2\dot{\mathbf{T}}_d \end{aligned} \tag{7}$$

where $\boldsymbol{w}_2 = {}^1\!/_2\mathbf{A}\Delta\boldsymbol{\rho}^2$ is a second set of lead factors and $\Delta\boldsymbol{\rho}^2 = [\Delta\rho_1^2, \Delta\rho_2^2, \ldots, \Delta\rho_M^2]^T$.

### B. Repolarization dispersion and lead factors

The approximation in equation (7) decomposes the surface T wave into a weighted sum of a function ($\mathbf{T}_d$) and its derivative. The weights $\boldsymbol{w}_1$ and $\boldsymbol{w}_2$ (the lead factors) depend directly on the transfer matrix $\mathbf{A}$ and on the repolarization times of the nodes (actually their deviations with respect to the average repolarization time).

One of the goals of this work is to show that, given the direct relation of the lead factors $\boldsymbol{w}_1$ and $\boldsymbol{w}_2$ with $\Delta\boldsymbol{\rho}$, it is possible to derive an estimate of the standard deviation $s_\vartheta$ of the instants $\rho_m$. This is a quantity which measures the dispersion of the repolarization times across the ventricles. The procedure is based on the definition of a stochastic (simplified) model for $\rho_m$. This is the first step in our reasoning.

[2]The minus sign was introduced to force the shape to be "upright" as the T-wave in most ECG standard leads is.

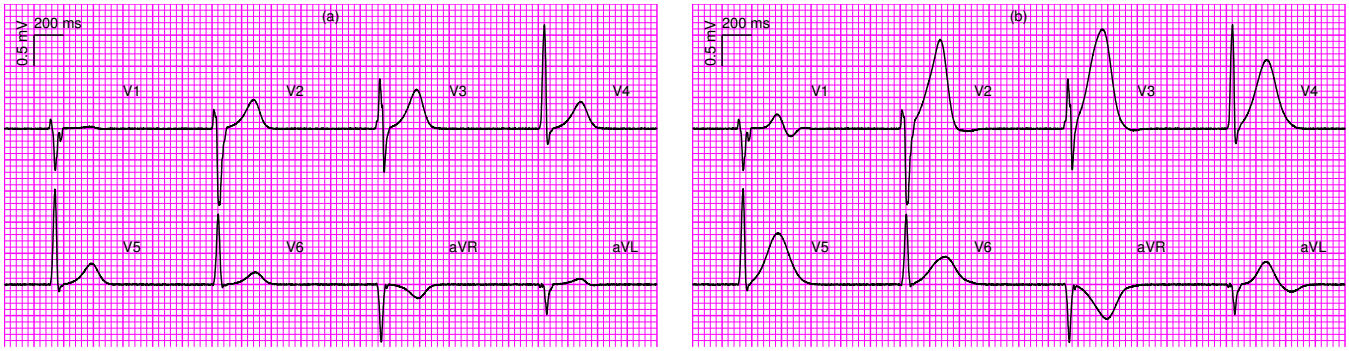


Fig. 1. Synthetic ECGs (leads V1 to V6, aVR and aVL) computed with the forward model in equation (3), the transmembrane potentials model of equation (18), the transfer matrix $\mathbf{A}$ and the repolarization times $\vartheta_m$ obtained from ECGSIM. Panel (a): $s_\vartheta = 20.6$ ms. Panel (b): $s_\vartheta = 70.9$ ms. In both cases, $\sigma_\varphi = 0$ ms and a 30 $\mu$V peak-to-valley broadband noise was added to mimic real ECGs. Note the peaking of the T–wave at higher dispersions of repolarization times.

## III. An estimate of the dispersion of repolarization times

### A. A simple model for the repolarization times $\rho_m$

Myocytes depolarization times $\delta_m$ are not random. The actual functioning of the cardiac pump requires that they do follow largely a physical time-sequence which is determined by the conduction path in the heart. A careful description of the isochronous activation lines in a healthy heart was provided by Durrer *et al.* [27]. Repolarization obviously takes place after depolarization. However, repolarization times do not necessarily follow the same isochronous activation lines. Moreover, while it is common to refer to a depolarization front moving along the myocardium, due to the slower change in the transmembrane potential, during repolarization the current density is dispersed across the entire ventricles. Therefore, the instant $\rho_m$ when the cell repolarizes is not so clearly defined as $\delta_m$. A common choice is to select it as the point of maximum downslope of the TMP.

The action potential duration (APD), $\rho_m - \delta_m$, displays its own spatial variability across the heart and it is not constant in time. An healthy subject will display a slight physiological variability across consecutive beats, while in pathological conditions (e.g. T-wave alternans) such variability might be greater. However, the dispersion around their average of the instants $\delta_m$ is smaller than the equivalent quantity computed for the times $\rho_m$.

Given this quickly-sketched scenario, a possible simple stochastic model for the repolarization time in one of the $M$ contiguous "nodes" in which the heart surface was subdivided, is

$$\rho_m(k) = \bar{\rho}(k) + \Delta\rho_m(k), \tag{8}$$

where the value $\bar{\rho}(k)$ is the average time of repolarization which might change with each beat $k$, while $\Delta\rho_m(k) \ll \bar{\rho}(k)$ is the deviation ("dispersion") with respect to the average value, with $\sum_{m=1}^{M} \Delta\rho_m(k) = 0$. Both terms are dependent on the current heart rate (HR): when HR increases, $\bar{\rho}(k)$ and $\Delta\rho_m(k)$ are expected to decrease. In order to avoid HR–related influences, we will limit our discussion to the case of stationary HR. In this situation, we subdivided $\Delta\rho_m(k)$ in two further terms:

$$\Delta\rho_m(k) = \vartheta_m + \varphi_m(k). \tag{9}$$

$\vartheta_m$ models the *spatial variability* of the repolarization times for a given subject, at a given HR. It is a function of the geometry of the heart, i.e. it takes into account the fact that repolarization starts at the bottom of the ventricles and moves up. $\varphi_m(k)$ describes the small, physiological differences in repolarization times which may occur among successive beats. In general it is reasonable to consider $\varphi_m(k) \ll \vartheta_m$, as discussed later. If pathological conditions affect the distribution of repolarization times, our model will describe it by a change in $\vartheta_m$. Recasting the problem from a signal processing point of view, $\vartheta_m$ is the main quantity we want to measure, while $\varphi_m(k)$ is a "noise" term which affects every measurement.

In the model, we take $\varphi_m(k)$ to be normally distributed as

$$\varphi_m(k) \sim \mathcal{N}(0, \sigma_\varphi^2(k)), \tag{10}$$

where the variance $\sigma_\varphi^2(k)$ is a function of the $k^{\text{th}}$ beat and the mean was set to zero with no lack of generality. In fact, any change in the average value of $\varphi$ is embedded in $\bar{\rho}(k)$ of Equation (8). The choice of a normal distribution is supported by the findings of Zaniboni *et al.* who studied: (i) the beat-to-beat $\text{APD}_{-60\text{mV}}$ in isolated rat ventricular myocytes, electrically stimulated at fixed pacing rates, and found that the distributions were normal, at any pacing rate [28]; (ii) the interbeat $\text{APD}_{90}$ (90% repolarization) distribution in guinea pig ventricular myocytes and found it was normally distributed [29]. Note that in (10) the variance $\sigma_\varphi^2(k)$ does not depend on $m$, as it is taken to be constant across the different zones of the heart. This is true only in first approximation, as slight differences were observed [26].

We also assume $\text{cov}[\varphi_i(k), \varphi_j(k)] = 0$ for $i \neq j$ and $\text{cov}[\varphi_i(k), \varphi_i(h)] = 0$ with $h \neq k$. That is the variations $\varphi(k)$ are independent random variables, both considering two distinct locations $(i, j)$ or the same node in two distinct beats $(k, h)$. These assumptions sound quite crude and deserve some comments. In fact, the study by [29] showed (and similar results were confirmed by other groups [30]) that when myocytes were coupled the APD standard deviation diminished. This is not in contrast with our hypothesis that

the random variables $\varphi_i$ are spatially uncorrelated as equation (10) describes the overall behavior of a "macroscopic" region of the heart, a node including several myocytes. That is, the term $\sigma_\varphi(k)$ already embeds the effects of local coupling with a nodal variability which is smaller then the variability of isolated myocardial cells.

Finally, when the variance of $\varphi_m(k)$ is constant among beats (and this is likely to happen in short time windows), we drop the explicit dependence on the beat number. Now, the deviations $\Delta\rho_m$ share the same standard deviation, hence

$$\Delta\rho_m \sim \mathcal{N}(\vartheta_m, \sigma_\varphi^2). \tag{11}$$

### B. Mean and variance of $\boldsymbol{w}_1$ and $\boldsymbol{w}_2$

For the second order approximation of $\boldsymbol{\Psi}$ given in equation (7) the lead factors corresponding to lead $i$ (with $i = 1, \ldots, L$ being $L$ the number of available leads) are

$$w_1(i) = -\sum_{m=1}^{M} A_{i,m}\Delta\rho_m \tag{12a}$$

$$w_2(i) = \frac{1}{2}\sum_{m=1}^{M} A_{i,m}\Delta\rho_m^2. \tag{12b}$$

From equations (11) and (12a), the quantity $w_1(i)$ is a normal random variable whose sample values can be obtained for each cardiac beat. Correspondingly, for the central limit theorem, when $M$ is large, $w_2(i)$ is approximatively normal.

Averaging in time, the moments of $w_1(i)$ are

$$E\left[w_1(i)\right] = -\sum_{m=1}^{M} A_{i,m}\vartheta_m \tag{13a}$$

$$\mathrm{var}\left[w_1(i)\right] = \sigma_\varphi^2 \sum_{m=1}^{M} A_{i,m}^2, \tag{13b}$$

which follows from the facts that: (i) when $M$ is large, $\sum_{m=1}^{M}[\vartheta_m + \varphi_m(k)] \approx \sum_{m=1}^{M}\vartheta_m = 0$; (ii) the normal distribution is stable; and (iii) $\mathrm{var}\left[\sum_{m=1}^{M} a_m X_m\right] = \sum_{i=m}^{M} a_m^2 \mathrm{var}\left[X_m\right]$ when $X_m$ are uncorrelated random variables [31]. In addition, recalling that $\sum_{m=1}^{M} A_{i,m} = 0$,

$$\begin{aligned} E\left[w_2(i)\right] &= \frac{1}{2}\sum_{m=1}^{M} A_{i,m} E\left[\Delta\rho_m^2\right] \\ &= \frac{1}{2}\sum_{m=1}^{M} A_{i,m}\left(\sigma_\varphi^2 + \vartheta_m^2\right) = \frac{1}{2}\sum_{m=1}^{M} A_{i,m}\vartheta_m^2. \end{aligned}$$

Finally, since for the normal random variable $\Delta\rho_m$ the (raw) moment $E\left[\Delta\rho_m^4\right] = \vartheta_m^4 + 6\vartheta_m^2\sigma_\varphi^2 + 3\sigma_\varphi^4$ [32, eq. 5-43 & 44],

$$\mathrm{var}\left[w_2(i)\right] = \frac{1}{4}\sum_{m=1}^{M} A_{i,m}^2 \mathrm{var}\left[\Delta\rho_m^2\right]$$

with

$$\mathrm{var}\left[\Delta\rho_m^2\right] = E\left[\Delta\rho_m^4\right] - \left(\sigma_\varphi^2 + \vartheta_m^2\right)^2 = 2\sigma_\varphi^4 + 4\sigma_\varphi^2\vartheta_m^2.$$

Hence

$$\mathrm{var}\left[w_2(i)\right] = \frac{\sigma_\varphi^4}{2}\sum_{m=1}^{M} A_{i,m}^2 + \sigma_\varphi^2 \sum_{m=1}^{M} A_{i,m}^2\vartheta_m^2. \tag{14}$$

### C. An assessment of the dispersion

The moments in equations (13b) and (14) depend on the elements of the transfer matrix $\mathbf{A}$ and on the deviations $\vartheta_m$, which are all unknown quantities. Taking their ratio, we have

$$\frac{\mathrm{var}\left[w_2(i)\right]}{\mathrm{var}\left[w_1(i)\right]} = \frac{\sigma_\varphi^2}{2} + \frac{\sum_{m=1}^{M} A_{i,m}^2\vartheta_m^2}{\sum_{m=1}^{M} A_{i,m}^2}. \tag{15}$$

With algebraic manipulations, the last sum in equation (14) can be rewritten as

$$\begin{aligned} \sum_{m=1}^{M} A_{i,m}^2\vartheta_m^2 = &\overbrace{\left(\sum_{m=1}^{M}\frac{\vartheta_m^2}{M}\right)}^{s_\vartheta^2}\left(\sum_{m=1}^{M} A_{i,m}^2\right) \\ &+ \underbrace{\sum_{m=1}^{M}\left(A_{i,m}^2 - \sum_{k=1}^{M}\frac{A_{i,k}^2}{M}\right)\left(\vartheta_m^2 - \sum_{k=1}^{M}\frac{\vartheta_k^2}{M}\right)}_{\mathcal{C}_i}, \end{aligned}$$

and using this expression into equation (15) we have

$$\frac{\mathrm{var}\left[w_2(i)\right]}{\mathrm{var}\left[w_1(i)\right]} = \frac{\sigma_\varphi^2}{2} + s_\vartheta^2 + \frac{\mathcal{C}_i}{\sum_{m=1}^{M} A_{i,m}^2}. \tag{16}$$

Let's focus on the three terms on the right hand side of equation (16). The value $s_\vartheta^2$ is an estimate of population variance of the set $\vartheta_m$ across the whole heart. It quantifies the *spatial* variability of the average repolarization times across different regions of the ventricles and it is constant across successive beats. In fact, in stationary conditions, the values $\vartheta_m$ are fixed in time for a given subject by definition (see section III-A). Chauhan *et al.* [26] showed that in healthy humans, the activation recovery interval (ARI) varies from about $220 \pm 17$ ms at the epicardium to about $250 \pm 10$ ms on the endocardium thus suggesting (for a healthy subject) a value of $s_\vartheta \approx 20$ ms across the ventricles.

On the other hand, $\sigma_\varphi$ measures the *temporal* variability of the physiological deviations $\Delta\rho_m$ at each node across successive beats. For the assumption we made in section III-A, it does not vary across the ventricles. The results of Zaniboni *et al.* hint that rat myocytes might display $\sigma_\varphi < 2$ ms at contraction rates $> 1$ Hz [28] which were further decreased by about 33% when cells were coupled. Walmsley *et al.* [30] found somewhat larger values for isolated myocytes from guinea pig hearts with $\sigma_\varphi \approx 4.1$ to $8.7$ ms. But they also confirmed that variability in ventricular preparations might be smaller than in isolated cells, as the interactions among myocytes have a stabilizing effect. Hence, $\sigma_\varphi < 4$ ms is a realistic value for *in vivo* human ventricular myocytes.

Finally, for each lead $i$, the third term can be rewritten as

$$\frac{\mathcal{C}_i}{\sum_{m=1}^{M} A_{i,m}^2} = \frac{\mathcal{C}_i}{M}\frac{M}{\sum_{m=1}^{M} A_i^2} = \frac{s_{(\vartheta^2, A_i^2)}}{s_{A_i}^2},$$

where $s_{(\vartheta^2, A_i^2)}$ is a measure of covariance between the (squared) deviations $\vartheta_m$ and the (squared) elements of the $i^{\mathrm{th}}$ line of the transfer matrix $\mathbf{A}$. $s_{A_i}^2$ is instead the variance of the elements composing the $i^{\mathrm{th}}$ line of the transfer matrix $\mathbf{A}$. Their ratio is a normalized measure of covariance and it is the only term, in equation (16), which depends on the lead $i$. Recalling

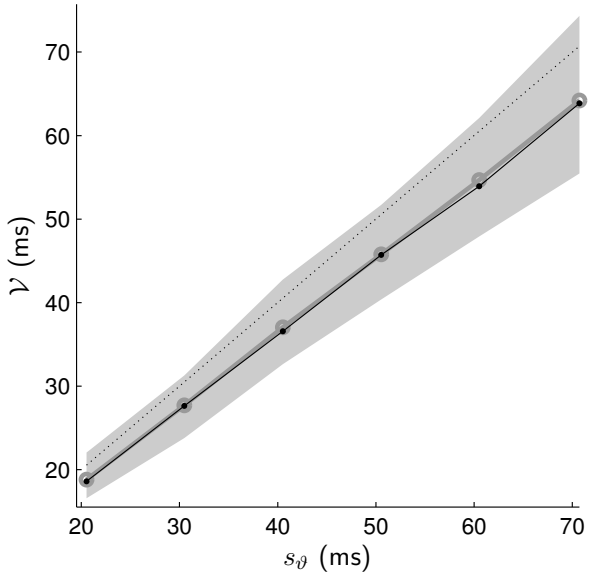


Fig. 2. Lead V3. Mean values (grey thick circles) and 95% confidence intervals (grey area) of the metric $\mathcal{V}$ for $\sigma_\varphi = 1$ ms computed on the exact values of $w_1(i)$ and $w_2(i)$ obtained from equations (12a) and (12b) on 128 "beats" (200 different runs were used to ensure statistical convergence of the confidence intervals). The picture also includes the quantities $[\sigma_\varphi^2 + s_\vartheta^2 + s_{(\vartheta^2,A_i^2)}/s_{A_i}^2]^{1/2}$, with $i$ corresponding to lead V3, (black dots connected by solid line) and $s_\vartheta$ (dotted line), for comparison.

that repolarization does not display a coherent temporal front, and that $M$ is large, we expect $s_{(\vartheta^2,A_i^2)}/s_{A_i}^2$ to be smaller than $s_\vartheta^2$. For example, for the data used next in section IV, the ratio $s_{(\vartheta^2,A_i^2)}/(s_{A_i}^2 s_\vartheta^2)$ is on average $-0.106 \pm 0.235$ across the 12 standard leads.

Given that $\sigma_\varphi \ll s_\vartheta$ and $s_{(\vartheta^2,A_i^2)}/s_{A_i}^2 \ll s_\vartheta^2$,

$$\mathcal{V}_i = \frac{\mathrm{std}\,[w_2(i)]}{\mathrm{std}\,[w_1(i)]} \approx s_\vartheta \tag{17}$$

provides an (approximate) measure of the dispersion of the average deviations $\Delta\rho_m$ across the ventricles. In first approximation, the quantity $\mathcal{V}_i$ is independent from the transfer matrix $\mathbf{A}$. Therefore it neither depends on the volume conductor nor the lead considered and we will refer to it as the "$\mathcal{V}$–index".

### *D. Practical notes*

Summarizing, the steps needed to compute the $\mathcal{V}$–index from a surface ECG recording are:

1) The model expects the heart rate to be stationary during the analysis, so ECG in controlled conditions should be obtained. After fiducial points detection and beats classification, the JT segment of each normal beat should be approximately located.
2) Values for $\mathbf{T}_d$, $\boldsymbol{w}_1$ and $\boldsymbol{w}_2$ should be estimated on the JT segment of each beat. Several approaches can be followed. We described the ones we selected for this work in Appendix A.
3) In each lead $i$, sample standard deviations are computed for the values of $w_1(i)$ and $w_2(i)$ obtained on consecutive beats. Then equation (17) is used to evaluate $\mathcal{V}_i$.
4) As $L$ different estimates are obtained, one for each lead, the consistency of the final $\mathcal{V}$–index can be increased by averaging them. A large number of leads is also useful to implicitly increase the consistency of the estimates of $\boldsymbol{w}_1$ and $\boldsymbol{w}_2$ as discussed in [33].

## IV. Test of the method on synthetic ECG

To provide a first assessment of the relation expressed in equation (17), a forward model for the electrical activity of the human heart in healthy conditions was employed. The forward model was described in equation (3) and we followed the implementation found in the ECGSIM software [34]. In practice, the heart surface is subdivided into 257 zones (42/54 representing the left/right endocardium, 61/70 the left/right epicardium and 14/16 the left/right septum) and in each one the myocytes are lumped into a single node. This means that, as a simplification, all the cells of a given node share the same transmembrane potential. To perform the simulations, we re-implemented the model within MATLAB (The MathWorks, Natick, MA) using the data and the forward transfer matrix $\mathbf{A}$ obtained from ECGSIM (version 1.3) and belonging to a healthy male individual [35]. In particular, within ECGSIM the standard deviation of the repolarization deviations $s_\vartheta$ was increased from the default values of 20.8 ms to 30.8, 40.8, 50.8, 60.8, and finally to 70.7 ms. This choice permits a direct comparison with the results in [15]. For each one of these 6 values, the set of transmembrane potentials was exported from ECGSIM and each potential (in mV) individually fitted (nonlinear least square) with the model [36]

$$S(t) = \gamma \overbrace{\frac{1}{1+e^{\alpha(t-\delta)}}}^{B(t-\delta)} \overbrace{\frac{1}{\left[1+e^{\beta_1(t-\rho)}\right]\left[1+e^{\beta_2(t-\rho)}\right]}}^{D(t-\rho)} - 100. \tag{18}$$

where $B(t-\delta)$ describes the depolarization part of the transmembrane potential and $D(t-\rho)$ the repolarization. The delay $\rho$ is approximatively the point at which $D(t-\rho)$ exhibits the largest negative slope[3] and we take it to be the repolarization time. The fitting of an analytical model refined slightly the positions of these repolarization times with respect to ECGSIM and, as a consequence, their standard deviation minimally changed. The actual values of $s_\vartheta$ used throughout the paper were: 20.6, 30.5, 40.6, 50.6, 60.6 and 70.9 ms.

To perform the actual simulations, for each of the 6 sets of ECGSIM repolarization deviations $\vartheta_m$, and for each value of $\sigma_\varphi$ in the range 0.1 to 100 ms, the instants $\rho_m$ were built using equation (9); then the transmembrane potential evaluated with equation (18) and sampled at 1000 Hz. Finally, using the linear forward transfer matrix $\mathbf{A}$, the electrical activities of the nodes were combined to provide the potentials at the locations of the 8 independent standard leads (V1–V6, aVR and aVL). Samples of the generated synthetic ECG signals are reported in figure (1). The procedure was repeated $K = 128$ times to mimic a sequence of consecutive beats, recorded with a stationary heart rate (for each one a different set of $\varphi_m$

[3]Actually the point of maximum negative slope is located at $t = \rho - \log(2)/\epsilon + o(\epsilon^3)$ where $\epsilon = (\beta_1 + \beta_2)/2$ does not depend on $\rho$.

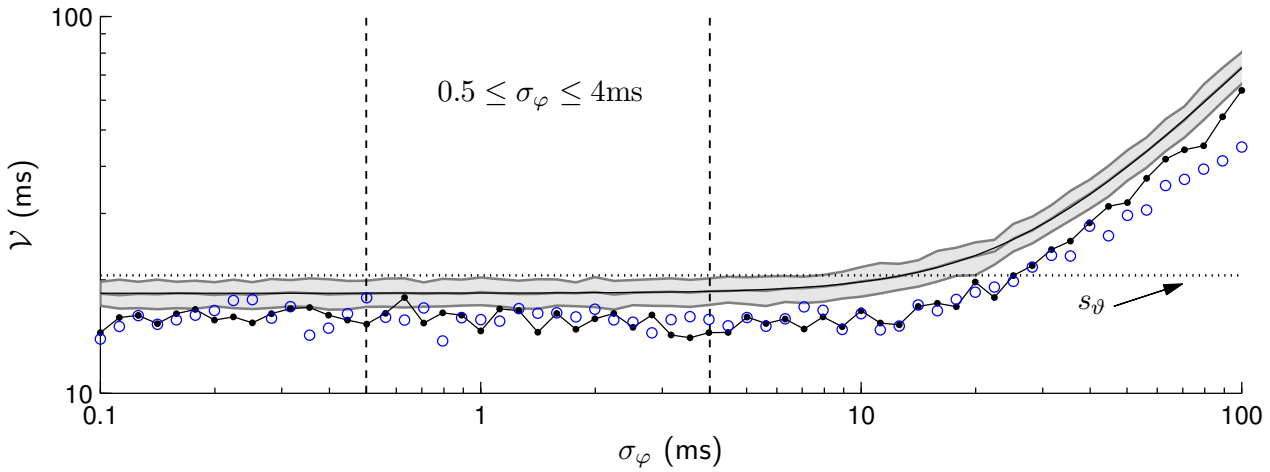


Fig. 3. The $\mathcal{V}$–index evaluated on 128 synthetic ECG beats constructed using equation (3). The deviations $\vartheta_m$ were obtained from ECGSIM with $s_\vartheta = 20.6$ ms while the values of $\varphi_m$ were drawn from a zero-mean normal distribution of variance $\sigma_\varphi^2$. No noise was added to the synthetic ECG for this computation. The lead factors were estimated: (i) with equation (27) (black dots •); and (ii) with equation (28) (empty circles ○). The picture contains the mean $\mathcal{V}$ values, averaged across the $L$ leads. The horizontal dotted line is set to the value $s_\vartheta = 20.6$. The grey area encloses the 95% confidence interval of the estimator $\mathcal{V}$ when computed on exact values of $\boldsymbol{w}_1$ and $\boldsymbol{w}_2$. The black continuous line marks the values computed from equation (16). For values of $\sigma_\varphi > 100$ ms third and higher order terms in equation (5) are generally not negligible and the approximation breaks down (not shown in picture).

was drawn from a normal distribution of standard deviation $\sigma_\varphi$). The number of consecutive beats, 128, was chosen to match the one used when testing for T wave alternans (TWA) with the spectral method [37], as commonly employed in the clinical routine. TWA is also supposed to arise from increased repolarization dispersion.

### *A. Validity of the approximation: an exact check*

As proof–of–concept, we first tested the validity of our derivation. Given the fact that, for each synthetic beat, the matrix $\mathbf{A}$ and the set of $\Delta\rho_m$ values were known, we computed the exact values for $\boldsymbol{w}_1$ and $\boldsymbol{w}_2$ as given in equations (12a) and (12b). Then, for each lead, these values were employed to estimate the $\mathcal{V}$–index, as defined in equation (17). Also we estimated the 95% confidence intervals of $\mathcal{V}$ with a Monte Carlo approach by repeating the procedure on 200 different runs of 128 synthetic beats each. The results are reported in figure (2) for lead V3.

According to the analytical reasoning of section III-C, the $\mathcal{V}$–index should match the square root of the quantity reported in equation (16). As shown in figure (2) this is actually the case: the average values estimated with the Monte Carlo procedure nearly overlap with the predictions of equation (16). We verified that this happened for every lead. As expected, the picture also makes clear that $\mathcal{V}$ is a biased estimator of $s_\vartheta$ (dotted line in the picture). The small bias is due to the fact that $\mathcal{V}$ is influenced by the normalized covariance $s_{(\vartheta^2,A_i^2)}/s_{A_i}^2$, which varies across leads.

### *B. Validity of the approximation: estimating the lead factors*

In practical situations, the lead factors are unfortunately unknown and must be estimated from the surface ECG. At this purpose, we described in the appendix A – see equation (27) – a technique we recently introduced [38] and that we further improved. Using the method, once picked out the JT segment from any of the 128 synthetic ECG beats, the lead factors $\boldsymbol{w}_1$ and $\boldsymbol{w}_2$ had been estimated for each lead simultaneously. Then the $\mathcal{V}$–index was computed across the 128 beats using equation (17) and averaged over the $L$ leads.

The results for $s_\vartheta = 20.6$ ms, are reported in figure (3) with black dots. For $\sigma_\varphi < 10$ ms the contribution of the interbeats variability to the final value of $\mathcal{V}$ is negligible as expected from equation (16) and section III-C. When $\sigma_\varphi$ grows further (even if this might not be significant from a physiological perspective), the values of $\mathcal{V}$ still follow the general behavior predicted by equation (16). On the other hand, the estimated $\mathcal{V}$ generally lies outside the 95% confidence interval obtained using the exact values of $w_1(i)$ and $w_2(i)$ in equations (12a) and (12b). That is, the numerical procedure which computes the lead factors from the surface ECG introduces a second source of bias. For example, in the physiologically relevant range $0.5 \leq \sigma_\varphi \leq 4$ ms, the average value of $\mathcal{V}$ obtained with the lead factors estimated from the synthetic ECGs is $15.6 \pm 1.0$ ms versus $18.4 \pm 0.8$ when computed with the exact values of $\boldsymbol{w}_1$ and $\boldsymbol{w}_2$.

The average values of $\mathcal{V}$ for $0.5 \leq \sigma_\varphi \leq 4$ ms obtained for different values of $s_\vartheta$ are included in figure (4). In these simulations, to increase the similarity with real ECGs, a 30 $\mu$V peak-to-valley broadband noise was added; the amplitude of the noise was selected to be the largest acceptable according to the IEC 60601-2-51 standard [39]. The metric evolves linearly with $s_\vartheta$ and the bias is larger than in figure (2) as noted in figure (3). This confirms that the bias introduced in the estimate of the terms $w_1(i)$ and $w_2(i)$ is larger than the one due to the covariance term in equation (16).

*Influence of the estimation method:* Given the fact that the method used to estimated $\boldsymbol{w}_1$ and $\boldsymbol{w}_2$ from the surface ECGs proved to be responsible for most of the bias, we tested two additional methods, also described in appendix A. The first is given by equation (28), and is by definition less

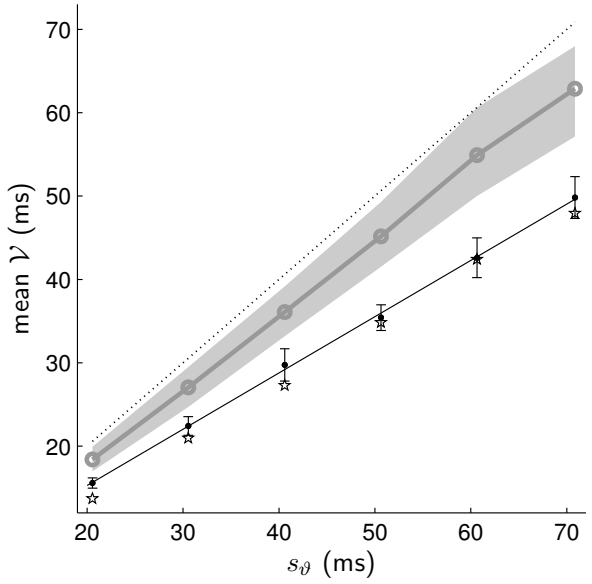


Fig. 4. Values of the mean $\mathcal{V}$–index computed for different sets $\vartheta_m$ obtained from ECGSIM (noise was added to the synthetic ECGs), averaged for $0.5 \leq \sigma_\varphi \leq 4$ ms (black dots, the error bars are twice the standard deviation long). The lead factors were estimated with equation (27). The regression line (continuous line) has equation $\mathcal{V} \approx 0.675\ s_\vartheta$ ($R^2 = 0.9992$). For a comparison, the line $\mathcal{V} = s_\vartheta$ is plotted as well (dotted line). The same average values of $\mathcal{V}$, but computed with the "basic" method of equation (28), are plotted with stars. The grey area is the 95% confidence interval of the average value of $\mathcal{V}$ when obtained from exact lead factors values as in figure 2 (but in there they were referred to the single lead V3).

accurate ("basic" approach). The results for $s_\vartheta = 20.6$ ms (empty circles) are included in figure (3). Surprisingly they are practically equivalent ($\mathcal{V} = 15.9 \pm 0.9$ ms) for small values of $\sigma_\varphi$. For $\sigma_\varphi > 10$ ms the technique is less effective, as the errors in the estimate of $\boldsymbol{w}_2$ build up and limit the accuracy of $\mathcal{V}$. On the other hand, when the ECG is noisy, the method selected to estimate the lead factors $\boldsymbol{w}_1$ and $\boldsymbol{w}_2$ plays a larger role. For example, the estimates of $\mathcal{V}$ computed using the "basic" approach are slightly less accurate, as figure (4) shows.

We also implemented a method which takes into account the third order derivative of $D(t)$ and is therefore more accurate. Nevertheless, the results are still equivalent[4] to the other ones for $\sigma_\varphi < 10$ ms, with only a limited reduction in the standard deviation of the estimates ($\mathcal{V} = 15.9 \pm 0.7$ ms).

## V. Test of the method on real ECGs

The tests performed on synthetic ECG signals were complemented by analysis on real ECG recordings. The experiments were performed on the E-OTH-12-0068-010 database, provided by the Telemetric and Holter ECG Warehouse of the University of Rochester (THEW), NY. The data were collected and previously analyzed by Kääb *et al.* [40]; please refer to their work for a complete description of the study protocol. Briefly, 17 patients were enrolled for documented torsades de pointes (TdPs) after administration of a drug with QT-prolonging potential. All patients tested positive for mutation of the major LQTS genes. A matched control group of 17 subjects was also enrolled and consisted of patients infused with sotalol for prevention of paroxysmal atrial fibrillation. At enrollment a baseline ambulatory ECG was recorded for each subject in supine position (12 standard leads, sampling rate: 1000 Hz, LSB: 5$\mu$V, duration: 95.6s or 218.5s for 17 cases each). Then, both groups were infused with a dose of 2mg/kg of sotalol, a drug known to prolong the QT interval, and a second ECG acquired at peak concentration of the drug.

The previous study of Kääb *et al.* showed that while the corrected QT (QTc, Bazett) was not significantly different across populations at enrollment (two sample t-test), it then differed after sotalol infusion. Also QTc differed significantly (paired t-test) within each population before and after infusion. While we do not have any clinical focus in here, the data permitted an indirect verification of the $\mathcal{V}$–index. In fact, while the repolarization deviations are unknown and a direct comparison is impossible, the QT prolongations after drug infusion should lead to an increased $s_\vartheta$ and then $\mathcal{V}$–index.

### A. Computational details

We selected the eight independent leads V1–V6, aVR and aVL, then each ECG in the E-OTH-12-0068-010 database went through a standard preprocessing. The first 10 seconds of each ECG were discarded to exclude boundary effects caused by the filter in the ECG device (affecting many recordings). Then band pass filtering was used to minimize baseline wandering and high-frequency disturbances. The filter had pass-bass $[0.05, 40]$ Hz ($3^{\text{rd}}$ order Butterworth filter) and was applied twice, after time reversal, to avoid any phase distortion. We employed the list of fiducial points supplied in the database. They were obtained from an automatic labeling software. To reduce the possibility of misclassifications, we built an average template using all the normal beats in the record and then marked as abnormal those ones which had a correlation factor with the template smaller than 0.9. The template was also used for a robust detection of the end of the QRS and T waves.

Finally, as the band-pass filtering imposed a zero DC component in each lead, a common baseline level was restored. This step showed to be critical. In fact, equation (7) does not contain any constant term to compensate from shifts in the DC component. While not theoretically relevant, this term could be added in the future to better suit practical situations.

The computation of the $\mathcal{V}$–index was performed as described in section III-D. In details, we extracted from each beat approximately the JT interval (plus 50 ms after the end of the T wave). As we were interested in the lead factors and not the dominant T wave itself, the exact location of the fiducial points was not necessary and a loose approximation sufficed (this is one of the advantages of the method). To avoid outliers due to artifact in the ECG, only those JT intervals where the DTW showed a cross-correlation larger than 0.9 with a common template were included in the computation of $\mathcal{V}_i$.

[4]When larger $\sigma_\varphi$ are considered, the third order method displays a larger accuracy in following the expected regime. While this follows from the theory, it is of limited practical use. For this reason we think that the increased numerical complexity of the third order method can be avoided in practical situations, at least in the current formulation.

The computed $\mathcal{V}$–index are reported in figure (5). The results matched the ones of Kääb *et al.*. The $\mathcal{V}$–index was not significantly different at enrollment between control and case group ($p = 0.11$ two samples t-test) while become significant after sotalol infusion ($p < 0.05$). Also the paired t-test within each group showed to be highly significant before and after drug infusion (for both $p < 0.01$). Out of 34 subjects, the $\mathcal{V}$–index increased in 30 ($p \ll 0.001$). Due to different ECG lengths and recording quality, for several records the metric was computed with a small number of beats (for 8 cases we used less than 64 beats, only 17 cases had at least 128 beats at disposal). The QTc values used in the previous study [40] were not available in the database, so a direct comparison could not be established.

## VI. Discussion and conclusion

In this work we proposed a method to estimate the standard deviation of the myocardial repolarization times from the surface ECGs. It is rooted into the surface source model which links the potential in a lead with the cellular transmembrane action potentials. Our work build on the concept of dominant T wave introduced by van Oosterom about a decade ago.

We verified, building synthetic ECG signals, that the analytical predictions of equation (16) were confirmed by numerical simulations. Also we showed that the $\mathcal{V}$–index scaled linearly with the standard deviation of the repolarization times $s_\vartheta$ ($R^2 = 0.9992$). This matched the results of Huysduynen *et al.* [15], where the indexes T-wave symmetry, T-wave amplitude[5] and T-wave area scaled linearly with $s_\vartheta$ in a related simulation. However, the $\mathcal{V}$–index represents a first attempts toward a direct measurement of $s_\vartheta$, while the others methods only provide an indirect assessment.

On the other hand, the simulations showed that the correlation terms in equation (16) and, more notably, the method used to estimate the lead factors $\boldsymbol{w}_1$ and $\boldsymbol{w}_2$ from the ECG, introduced a bias in $\mathcal{V}$. While this is unavoidable at the moment, more research should be envisioned in increasing the reliability of these estimates – for example exploring a parametric description for $\mathbf{T}_d$ as suggested in [42].

Finally, the tests made on the real ECG recordings, showed that the $\mathcal{V}$–index, while needing improvements and further development for practical applications, provided estimates of the standard deviation of the repolarization times which were reasonable and which paired with what expected from the previous study of Kääb *et al.* on the same data.

Concluding, the $\mathcal{V}$ index might provide a measure of the repolarization dispersion from the surface ECG clearly linked to a recognized electrophysiological model.

[5]A larger heterogeneity of repolarization times is known to increase the amplitude of the T waves, i.e. see figure (1). So, it comes natural to question if the differences noticed by Kääb and coworkers, and confirmed by the $\mathcal{V}$ index in here, could have been detected simply comparing the amplitudes of the T waves. This becomes even more intriguing after noticing that, in the JT interval, $\max_j \psi_{i,j} \approx w_1(i) \max_j T_d(j)$. To check this idea, for each ECG, we computed the root mean square curve, i.e. $\mathrm{RMS}(j) \approx T_d(j) \left[\sum_{i=1}^{L} w_1^2(i)/L\right]^{1/2}$ as in [18], and located its maximum value in every JT interval. The median of these maxima, once compared between the different groups of patients, never turned out to be significantly different (*t*-test). This is consistent with the fact that effects of sotalol on T wave amplitudes were shown to appear only at higher doses or later in time [41].

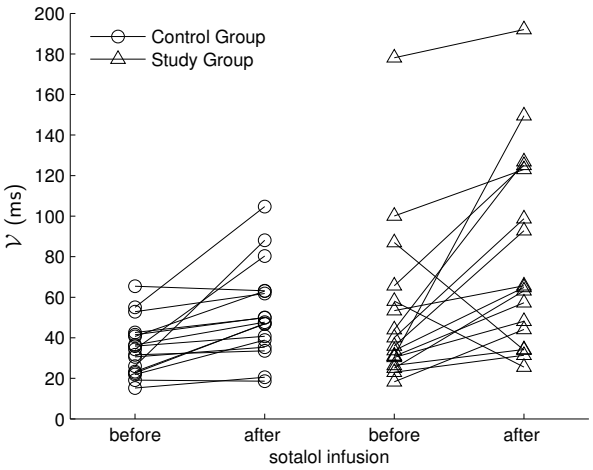


Fig. 5. The values of the $\mathcal{V}$–index computed on the ECG recordings of the THEW's E-OTH-12-0068-010 database. Please refer to section V for details. The average values of $\mathcal{V}$ were: for the control group, $\mathcal{V} = 35.0 \pm 13.7$ ms (before sotalol infusion) and $\mathcal{V} = 52.4 \pm 22.8$ ms (after sotalol infusion); for the study group, $\mathcal{V} = 51.8 \pm 39.7$ ms (before) and $\mathcal{V} = 81.0 \pm 48.1$ ms (after). Overall, for the entire population $\mathcal{V} = 43.4 \pm 30.4$ ms (before) and $\mathcal{V} = 66.7 \pm 39.8$ ms (after).

## Appendix A
## Estimates of the DTW and the lead factors

### A. First order approximation of $D(t)$

Van Oosterom mentioned two different ways to estimate $\mathbf{T}_d$. Initially he suggested [25] the average of the potentials in $\boldsymbol{\Psi}$ weighted by their integrals $\mathbf{e}_1^T \boldsymbol{\Psi}^T$, that is[6]

$$\mathbf{T}_d = c_1 \mathbf{e}_1^T \boldsymbol{\Psi}^T \boldsymbol{\Psi}. \tag{19}$$

Implicitly he implied that

$$\boldsymbol{w}_1 = \frac{\boldsymbol{\Psi}\mathbf{e}_1}{\mathbf{T}_d \mathbf{e}_1}.$$

Soon after, observing that the series expansion implied by equations (4) and (5) is a composition of rank-1 matrixes, with some resemblances with the more classical rank-1 decomposition obtained through singular value decomposition (SVD),

$$\boldsymbol{\Psi} = \mathbf{U}\boldsymbol{\Lambda}\mathbf{V}^T = \sum_{i=1}^{L} \mathbf{u}_i \lambda_i \mathbf{v}_i^T.$$

he hinted [43] to an estimate for $\mathbf{T}_d$ obtained also with

$$\mathbf{T}_d = c_2 \lambda_1 \mathbf{v}_1^T \tag{20a}$$

$$\boldsymbol{w}_1 = \frac{\mathbf{u}_1}{c_2}. \tag{20b}$$

Similarly, in [42], $\mathbf{T}_d$ was computed through principal component analysis (PCA) as

$$\mathbf{T}_d = c_3 \boldsymbol{\zeta}_1^T \boldsymbol{\Psi} \tag{21}$$

[6]In equations (19), (20a) and (21), the scalars $c_1$, $c_2$ and $c_3$ are set so that the integral of $T_d(t)$

$$-\int_{t_{\mathrm{de}}}^{t_{\mathrm{re}}} T_d(\tau)\, \mathrm{d}\tau \approx 100$$

evaluates to the average difference in the intracellular potential before ($t_{\mathrm{de}}$) and after repolarization ($t_{\mathrm{re}}$), e.g. 100 mV.

where $\boldsymbol{\zeta}_1$ is the $[L\times 1]$ eigenvector of the inter-leads covariance matrix $\boldsymbol{\Psi}\left(\mathbf{I}-\mathbf{e}_1\mathbf{e}_1^T/N\right)\boldsymbol{\Psi}^T$ associated to the largest eigenvalue. But $\boldsymbol{\zeta}_1 \approx \mathbf{u}_1$ and the two estimates in equations (20a) and (21) are nearly identical.

When the singular value $\lambda_1 \gg \lambda_{i\neq 1}$, even the two equations (19) and (20a) produce very similar values. In fact,

$$\boldsymbol{\Psi}^T\boldsymbol{\Psi} = \mathbf{V}\boldsymbol{\Lambda}^2\mathbf{V}^T = \sum_{i=1}^{L}\lambda_i^2\mathbf{v}_i\mathbf{v}_i^T,$$

hence

$$\mathbf{e}_1^T\boldsymbol{\Psi}^T\boldsymbol{\Psi} = \sum_{i=1}^{L}(\lambda_i^2\mathbf{e}_1^T\mathbf{v}_i)\mathbf{v}_i^T \approx (\lambda_1^2\mathbf{e}_1^T\mathbf{v}_1)\mathbf{v}_1^T.$$

However, as shown in [33], the estimate in equation (20a) is *optimal* in the sense that it minimizes the Frobenius norm of the quadratic error

$$\epsilon = \|\boldsymbol{\Psi} - \boldsymbol{w}_1\mathbf{T}_d\|_F, \tag{22}$$

thus offers the best rank$-1$ approximation to the matrix of the surface potentials.

### *B. Higher order approximation of $D(t)$*

Lemay *et al.* [42] first suggested a technique to estimate the DTW taking into account higher order derivatives of $D(t)$. The procedure was two-steps. Initially $\mathbf{T}_d$ was estimated with equation (19) and further approximated by fitting a smooth analytical function with continuous derivatives (this decreases the noise injected into the problem). Afterwards the lead factors were computed with a linear parameter estimation problem. The authors verified that fourth and higher-order components of $D(t)$ could hardly be distinguished from noise. The focus of the procedure was on the DTW only, though, and not on the lead factors.

A minimization of the Frobenius norm of the residual matrix, similar to equation (22), is commonly pursued in inverse electrocardiography. Coherently with this perspective, in a preliminary research [38], we suggested to compute simultaneously $\mathbf{T}_d$, $\boldsymbol{w}_1$ and $\boldsymbol{w}_2$ by minimizing

$$\epsilon = \|\boldsymbol{\Psi} - \boldsymbol{w}_1\mathbf{T}_d - \boldsymbol{w}_2\dot{\mathbf{T}}_d\|_F. \tag{23}$$

The procedure was based on a finite difference numerical approximation of $\mathbf{T}_d$ and, for $s_\vartheta$ in the range 10 to 50 ms, it demonstrated to be an improvement over previous methods.

A procedure, which offers further improvements, was developed and employed for this paper. We alternatively minimized the functional

$$\hat{\epsilon}^2 = \sum_{i=1}^{L}\int_{\mathrm{JT}}\left[\Psi_i(t) - w_1(i)T_d(t) - w_2(i)\dot{T}_d(t)\right]^2\mathrm{d}t, \tag{24}$$

which is a continuous-time extension of equation (23). A classical result [44] states that the minimum of (24) is reached for a function $T_d(t)$ which solves the Euler-Lagrange equation

$$T_d(t)\sum_{i=1}^{L}w_1^2(i) - \ddot{T}_d(t)\sum_{i=1}^{L}w_2^2(i) = \\ = \sum_{i=1}^{L}w_1(i)\Psi_i(t) - \sum_{i=1}^{L}w_2(i)\dot{\Psi}_i(t)$$

along with the conditions of transversality at the free borders

$$T_d(t)\sum_{i=1}^{L}w_1(i)w_2(i) + \dot{T}_d(t)\sum_{i=1}^{L}w_2^2(i) = \sum_{i=1}^{L}w_2(i)\Psi_i(t).$$

Then a second-order finite difference approximation leads to

$$\begin{aligned} &T_d(j)\left[\|\boldsymbol{w}_1\|^2 + 2\|\boldsymbol{w}_2\|^2/(\Delta t)^2\right] \\ &\quad - \left[T_d(j+1) + T_d(j-1)\right]\|\boldsymbol{w}_2\|^2/(\Delta t)^2 = \\ &\quad \sum_{i=1}^{L}\left\{\Psi_{i,j}w_1(i) - \left[\Psi_{i,j+1} - \Psi_{i,j-1}\right]w_2(i)/(2\Delta t)\right\}, \end{aligned} \tag{25}$$

where $\Delta t$ is the inverse of the sampling rate, with

$$\dot{T}_d(j) = -\frac{\sum_{i=1}^{L}\left[T_d(j)w_1(i)w_2(i) - w_2(i)\Psi_{i,k}\right]}{\sum_{i=1}^{L}w_2^2(i)} \tag{26}$$

for $j = 1$ and $N$. Summarizing, an estimate for $\boldsymbol{w}_1$ and $\boldsymbol{w}_2$ is computed first by solving

$$\begin{cases} \boldsymbol{w}_1\|\mathbf{T}_d\|^2 + \boldsymbol{w}_2\dot{\mathbf{T}}_d\mathbf{T}_d^T = \boldsymbol{\Psi}\mathbf{T}_d^T \\ \boldsymbol{w}_1\dot{\mathbf{T}}_d\mathbf{T}_d^T + \boldsymbol{w}_2\|\dot{\mathbf{T}}_d\|^2 = \boldsymbol{\Psi}\dot{\mathbf{T}}_d{}^T. \end{cases} \tag{27}$$

Then a new value for $\mathbf{T}_d$ is obtained from equations (25)-(26) and the two steps are iterated. We verified that 3 iterations (which we employed consistently) grant, on average, an error on the estimates smaller that $1\%$. The numerical procedure is overall computationally efficient as it (approximatively) minimizes the nonlinear functional by solving two linear banded-diagonal systems of equations. Along these lines we also built an estimate of $\boldsymbol{w}_1$ and $\boldsymbol{w}_2$ which takes into account the third order derivative of $D(t)$. It requires an extension to the classical Euler-Lagrange equation [44].

A simpler and less effective technique is the one we termed as "basic" in this paper. The lead factors are obtained via successive reduction of the Frobenius norm. First both $\mathbf{T}_d$ and $\boldsymbol{w}_1$ are obtained with equations (20a)-(20b) and $\dot{T}_d(j) = [T_d(j+1) - T_d(j-1)]/(2\Delta)$. Then $\boldsymbol{w}_2$ is forced to minimize the residual

$$\epsilon = \|\Upsilon - \boldsymbol{w}_2\dot{\mathbf{T}}_d\|_F,$$

where $\Upsilon = \boldsymbol{\Psi} - \boldsymbol{w}_1\mathbf{T}_d$. That is,

$$\boldsymbol{w}_2 = \frac{\Upsilon\dot{\mathbf{T}}_d}{\|\dot{\mathbf{T}}_d\|^2}. \tag{28}$$

The "basic" estimates were used in our code (which is available under request from the authors) to start the iteration in equation (27).

As a final note, we acknowledge that the methods described share the separate evaluation of $\boldsymbol{w}_1$ and $\boldsymbol{w}_2$. This might seem questionable as both quantities depend on $\Delta\boldsymbol{\rho}$. On the other hand, this appears reasonable if one considers that the large number of sources in $\Delta\boldsymbol{\rho}$ makes $\boldsymbol{w}_1$ and $\boldsymbol{w}_2$ *practically* uncorrelated.

## ACKNOWLEDGMENT

Data used for this research were provided by the Telemetric and Holter ECG Warehouse of the University of Rochester (THEW), NY. The authors express their gratitude to the THEW initiative. RS would also like to thank Thom Oostendorp and Peter van Dam for clarifications on the ECGSIM software.

## REFERENCES


[1] C. S. Kuo, K. Munakata, C. P. Reddy, and B. Surawicz, "Characteristics and possible mechanism of ventricular arrhythmia dependent on the dispersion of action potential durations." *Circulation*, vol. 67, no. 6, pp. 1356–1367, 1983.

[2] J. A. Vassallo, D. M. Cassidy, K. E. Kindwall, F. E. Marchlinski, and M. E. Josephson, "Nonuniform recovery of excitability in the left ventricle." *Circulation*, vol. 78, no. 6, pp. 1365–1372, 1988.

[3] L. D. Ambroggi, "Heterogeneities of ventricular repolarization and vulnerability to arrhythmia. How to detect them with noninvasive methods?" *Cardiologia*, vol. 44, no. 4, pp. 355–360, 1999.

[4] M. Malik, "Nondipolar electrocardiographic components and myocardial heterogeneity." *Ann Noninvasive Electrocardiol*, vol. 14, no. 2, pp. 103–107, 2009.

[5] P. D. Arini, G. C. Bertrán, E. R. Valverde, and P. Laguna, "T-wave width as an index for quantification of ventricular repolarization dispersion: Evaluation in an isolated rabbit heart model," *Biomedical Signal Processing and Control*, vol. 3, pp. 67–77, 2008.

[6] M. Kesek, O. Gustavsson, and U. Wiklund, "Nondipolar content of T wave derived from a myocardial source simulation with increased repolarization inhomogeneity." *Ann Noninvasive Electrocardiol*, vol. 14, no. 2, pp. 185–192, 2009.

[7] C. P. Day, J. M. McComb, and R. W. Campbell, "QT dispersion: an indication of arrhythmia risk in patients with long qt intervals." *Br Heart J*, vol. 63, no. 6, pp. 342–344, 1990.

[8] G. X. Yan and C. Antzelevitch, "Cellular basis for the normal T wave and the electrocardiographic manifestations of the long-QT syndrome." *Circulation*, vol. 98, no. 18, pp. 1928–1936, 1998.

[9] A. Mincholé, E. Pueyo, J. F. Rodríguez, E. Zacur, M. Doblaré, and P. Laguna, "Quantification of restitution dispersion from the dynamic changes of the t-wave peak to end, measured at the surface ecg." *IEEE Trans Biomed Eng*, vol. 58, no. 5, pp. 1172–1182, 2011.

[10] C. Antzelevitch, S. Sicouri, J. M. D. Diego, A. Burashnikov, S. Viskin, W. Shimizu, G.-X. Yan, P. Kowey, and L. Zhang, "Does Tpeak-Tend provide an index of transmural dispersion of repolarization?" *Heart Rhythm*, vol. 4, no. 8, pp. 1114–6; author reply 1116–9, 2007.

[11] W. Zareba, "Dispersion of repolarization: Time to move beyond QT dispersion," *Ann Noninvasive Electrocardiol*, vol. 5, pp. 373–381, 2000.

[12] A. J. Moss, "What resides in T-wave residuum?" *J Cardiovasc Electrophysiol*, vol. 16, no. 9, pp. 952–953, 2005.

[13] T. Opthof, R. Coronel, F. J. G. Wilms-Schopman, A. N. Plotnikov, I. N. Shlapakova, P. Danilo, M. R. Rosen, and M. J. Janse, "Dispersion of repolarization in canine ventricle and the electrocardiographic t wave: Tp-e interval does not reflect transmural dispersion." *Heart Rhythm*, vol. 4, no. 3, pp. 341–348, 2007.

[14] Y. Xia, Y. Liang, O. Kongstad, Q. Liao, M. Holm, B. Olsson, and S. Yuan, "In vivo validation of the coincidence of the peak and end of the T wave with full repolarization of the epicardium and endocardium in swine." *Heart Rhythm*, vol. 2, no. 2, pp. 162–169, 2005.

[15] B. H. V. Huysduynen, C. A. Swenne, H. H. M. Draisma, M. L. Antoni, H. V. D. Vooren, E. E. V. D. Wall, and M. J. Schalij, "Validation of ECG indices of ventricular repolarization heterogeneity: a computer simulation study." *J Cardiovasc Electrophysiol*, vol. 16, no. 10, pp. 1097–1103, 2005.

[16] D. B. Geselowitz, "Description of cardiac sources in anisotropic cardiac muscle. Application of bidomain model," *Journal of Electrocardiology*, vol. 25, no. Supplement 1, pp. 65 – 67, 1992.

[17] A. van Oosterom, "Genesis of the T wave as based on an equivalent surface source model," *J Electrocardiol*, vol. 34 Suppl, pp. 217–227, 2001.

[18] ——, "The dominant T wave," *J Electrocardiol*, vol. 37 Suppl, pp. 193–197, 2004.

[19] W. Miller and D. Geselowitz, "Simulation studies of the electrocardiogram. I. The normal heart," *Circ Res*, vol. 43, no. 2, pp. 301–315, 1978.

[20] L. Tung, "A bi-domain model for describing ischemic myocardial D-C potentials," Ph.D. thesis, Massachusetts Institute of Technology. Dept. of Electrical Engineering and Computer Science, 1978.

[21] O. H. Schmitt, *Information Processing in the Nervous System*. Springer-Verlag, New York, 1969, ch. Biological information processing using the concept of interpenetrating domains, pp. 325–331.

[22] S. Scacchi, P. C. Franzone, L. Pavarino, and B. Taccardi, "A reliability analysis of cardiac repolarization time markers," *Mathematical Biosciences*, vol. 219, no. 2, pp. 113 – 128, 2009.

[23] D. B. Geselowitz, "On the theory of the electrocardiogram," *Proc. IEEE*, vol. 77, pp. 857–876, 1989.

[24] R. Plonsey and R. C. Barr, "Current flow patterns in two-dimensional anisotropic bisyncytia with normal and extreme conductivities," *Biophys J.*, vol. 45, no. 3, pp. 557–571, 1984.

[25] A. van Oosterom, "The dominant T wave and its significance," *J. Cardiovasc. Electrophysiol.*, vol. 14, pp. S180–187, 2003.

[26] V. S. Chauhan, E. Downar, K. Nanthakumar, J. D. Parker, H. J. Ross, W. Chan, and P. Picton, "Increased ventricular repolarization heterogeneity in patients with ventricular arrhythmia vulnerability and cardiomyopathy: a human in vivo study," *Am. J. Physiol. Heart Circ. Physiol.*, vol. 290, pp. 79–86, 2006.

[27] D. Durrer, R. T. v. Dam, G. E. Freud, M. J. Janse, F. L. Meijler, and R. C. Arzbaecher, "Total excitation of the isolated human heart," *Circulation*, vol. 41, pp. 899–912, 1970.

[28] M. Zaniboni, F. Cacciani, and N. Salvarani, "Temporal variability of repolarization in rat ventricular myocytes paced with time-varying frequencies," *Experimental Physiology*, vol. 92, no. 5, pp. 859–869, 2007.

[29] M. Zaniboni, A. E. Pollard, L. Yang, and K. W. Spitzer, "Beat-to-beat repolarization variability in ventricular myocytes and its suppression by electrical coupling," *Am. J. Physiol. Heart Circ. Physiol.*, vol. 278, no. 3, pp. H677–H687, 2000.

[30] J. Walmsley, G. Mirams, M. Bahoshy, C. Bollensdorff, B. Rodriguez, and K. Burrage, "Phenomenological modeling of cell-to-cell and beat-to-beat variability in isolated Guinea Pig ventricular myocytes," in *Conf Proc IEEE Eng Med Biol Soc*, vol. 1, 2010, pp. 1457–1460.

[31] A. M. Mood, F. A. Graybill, and D. C. Boes, *Introduction to the Theory of Statistics*, 3rd ed. McGraw-Hill Publishing Co., 1974.

[32] A. Papoulis, *Probability, Random Variables, and Stochastic Processes*, 3rd ed. New York: McGraw-Hill, 1991.

[33] L. T. Mainardi and R. Sassi, "Analysis of T Wave Alternans using the Dominant T-wave paradigm," *Journal of Electrocardiology*, vol. 44, pp. 119–125, 2011.

[34] A. van Oosterom and T. F. Oostendorp, "ECGSIM: an interactive tool for studying the genesis of QRST waveforms," *Heart*, vol. 90, pp. 165–168, 2004.

[35] A. van Oosterom and G. J. Huiskamp, "The effect of torso inhomogeneities on body surface potentials quantified using "tailored" geometry," *J Electrocardiol*, vol. 22, pp. 53–72, 1989.

[36] P. van Dam, T. Oostendorp, A. Linnenbank, and A. van Oosterom, "Non-invasive imaging of cardiac activation and recovery," *Annals of Biomedical Engineering*, vol. 37, pp. 1739–1756, 2009.

[37] J. Smith, E. Clancy, C. Valeri, J. Ruskin, and R. Cohen, "Electrical alternans and cardiac electrical instability," *Circulation*, vol. 77, no. 1, pp. 110–121, 1988.

[38] R. Sassi and L. T. Mainardi, "Refined estimate of the dominant T-wave," in *Computers in Cardiology, 2010*, vol. 37, 2010, pp. 845–848.

[39] IEC 60601-2-51 Standard, "Medical electrical equipment - part 2-51: Particular requirements for safety, including essential performance, of recording and analysing single channel and multichannel electrocardiographs," 2003.

[40] S. Kääb, M. Hinterseer, M. Näbauer, and G. Steinbeck, "Sotalol testing unmasks altered repolarization in patients with suspected acquired long-QT-syndrome—a case-control pilot study using i.v. sotalol," *European Heart Journal*, vol. 24, no. 7, pp. 649–657, 2003.

[41] F. Extramiana, R. Dubois, M. Vaglio, P. Roussel, G. Dreyfus, F. Badilini, A. Leenhardt, and P. Maison-Blanche, "The time course of new t-wave ECG descriptors following single- and double-dose administration of sotalol in healthy subjects," *Ann Noninvasive Electrocardiol*, vol. 15, no. 1, pp. 26–35, 2010.

[42] M. Lemay, J. M. Vesin, A. van Oosterom, V. Jacquemet, and L. Kappenberger, "Cancellation of ventricular activity in the ECG: evaluation of novel and existing methods," *IEEE Trans Biomed Eng*, vol. 54, pp. 542–546, 2007.

[43] A. van Oosterom, "Singular value decomposition of the T wave: Its link with a biophysical model of repolarization," *Int. J. Bioelectromagnetism*, vol. 4, pp. 59–60, 2002.

[44] G. Barbero and L. R. Evangelista, *An Elementary Course on the Continuum Theory for Nematic Liquid Crystals*. World Scientific, 2000.